Slow and fast light associated with polariton interference

B. Gu,[1] N. H. Kwong,[2] R. Binder,[1,2] and Arthur L. Smirl[3]

[1]*Department of Physics, University of Arizona, Tucson, Arizona 85721, USA*

[2]*College of Optical Sciences, University of Arizona, Tucson, Arizona 85721, USA*

[3]*Laboratory for Photonics and Quantum Electronics, University of Iowa, Iowa City, Iowa 52242, USA*

Propagation times of optical pulses through a medium near an absorptive resonance with and without spatial dispersion are studied and contrasted. When spatial dispersion is not present, a light pulse is expected to traverse a medium in a time inversely proportional to its group velocity. In a medium with spatial dispersion, where two polariton modes exist (here, bulk GaAs as an example), a similar description is obtained if the losses are such that light propagates primarily in one mode. However, we show that, when the broadening of the resonance (dephasing rate) is below a critical value, a frequency range exists near resonance where the transit times are determined by interference between copropagating polaritons and deviate strongly from expectations based on the group velocities of the polariton branches. When the interference is constructive at the samples end face, the transit times are determined by the average of the inverse group velocities; when it is destructive, we find abrupt transitions between very slow (long positive) and very fast (large negative) transit times. We present quantitative criteria for the resolution of these features and for distortion-free propagation in the spectral vicinity of them. Our analysis puts the well-known slow- and fast-light effects in systems without spatial dispersion into a broader context by illustrating that they are a limiting case of systems with spatial dispersion.

PACS number(s): 71.36.+c, 42.25.Bs, 78.40.Fy

I. INTRODUCTION

Over the past decade, interest in controlling the velocity of light pulses has been renewed, in part because of potential applications in telecommunications, spectroscopy, and so-called microwave photonics (for recent introductions and reviews see Refs. 1 and 2). Studies have shown that the interaction of light with matter can lead to extreme changes in the effective or apparent velocities of pulses of light: for example, pulse envelopes that travel a few meters per second,[3] that appear to exit the material before the peaks of the pulses enter it,[4–10] and that appear to travel backward in the material[8] have been reported. These phenomena have been investigated in media ranging from atomic vapors[3,11–13] to solid materials, such as doped crystals,[14] optical fibers,[15,16] and semiconductors (doped,[4] bulk,[17] and quantum wells[18]). Most recent schemes for producing slow, fast or backward traveling light take advantage of sharp resonances in nonlinear processes, such as electromagnetically induced transparency,[3] stimulated Brillouin scattering,[15,16] or coherent population oscillations.[8,14,19–21]

The simplest demonstration of slow (subluminal) and fast (superluminal) light propagation, however, is the *linear* interaction of a light pulse with an absorptive medium consisting of identical, localized dipole oscillators. This topic has been considered for almost a century[22] and is commonly addressed in text books.[23] In the absence of interactions between the two (and in the absence of losses), the light and oscillator have independent dispersion relations (frequency vs wave vector) given by $\omega(k)=ck$ and $\omega(k)=E_x/\hbar$, respectively, as sketched in Fig. 1(a). As we discuss in the next section, for pulses that have a sufficiently narrow spectral width, the pulse envelope is transmitted undistorted with a group velocity v_g.

Most conventional descriptions of light propagating near a resonance neglect direct coupling between the dipole oscillators (i.e., they are only coupled indirectly through their interaction with the same light field). If present, electronic coupling will allow the light-induced optical polarization (exciton) to move through the system. This motion can be included through the kinetic energy of the optical polarization, $\hbar^2 k^2/2M_x$, where M_x is the effective mass of the polarization. Figure 1(b) shows a sketch of the uncoupled material and light dispersions for $M_x<\infty$. The case of vanishing elec-
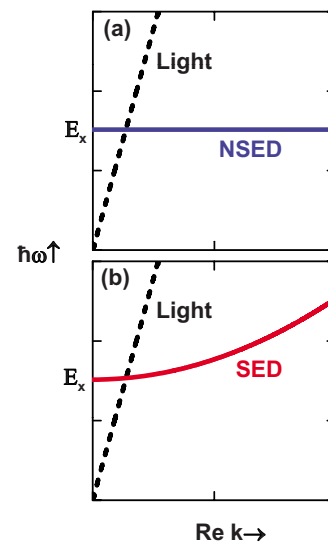

FIG. 1. (Color online) Sketch of the uncoupled (and unbroadened) exciton and photon-dispersion relations (with real ω and real k) for two exciton masses: (a) $M_x=\infty$, labeled NSED for no spatial exciton dispersion and (b) $M_x<\infty$ labeled SED for spatial exciton dispersion.

tronic coupling should be recovered by allowing the effective mass to become arbitrarily large ($M_x \rightarrow \infty$). The limit of $M_x = \infty$ (i.e., $M_x^{-1} = 0$) is implicitly assumed in much of the slow- and fast-light literature (e.g., Refs. 4, 6–8, and 24), so it is natural to ask whether removing this restriction by allowing $M_x < \infty$ causes nontrivial modifications in the slow- and fast-light behavior. In fact, here, we show that we can find certain frequencies (close to the exciton resonance) where the time delay cannot be explained in terms of the concept of a group velocity (no matter how narrow the bandwidth). Furthermore, we find infinities in the delay times that are absent when $M_x = \infty$. Since $M_x = \infty$ is just a limiting case of $M_x < \infty$, it seems important to have a unified model that provides for an understanding of the slow- and fast-light characteristics in each regime and shows how features in the $M_x < \infty$ case collapse into the well-studied $M_x = \infty$ case.

In Sec. II, we review the well-known exciton-polariton dispersion relation and the transmission coefficients of semiconductor slabs with finite thicknesses, focusing on the difference between $M_x < \infty$ and $M_x = \infty$. In doing so, we define a critical dephasing rate, below which the polariton interference effects may be important. In Sec. III, we present the definition of transit time to be used in our analyses and in Sec. IV, we pedagogically describe polariton interference effects for spectrally narrow pulses using an intuitive two-wave (TW) model. In Sec. V we define more precisely what we mean by "spectrally narrow" and consider the effects of non-negligible spectral widths on the pulse transit times near spectral features produced by polariton interference. Finally, in Sec. V, we comment on the pulse deformations that can accompany polariton interference effects.

II. POLARITON DISPERSION

Here, we provide a brief review of the well-known (e.g., Refs. 24–27) linear optical properties of coupled exciton-light modes (polaritons) needed for the analysis of slow- and fast-light presented below. To be specific, we use exciton polaritons in bulk semiconductors as an example: $M_x < \infty$ corresponds to the unbound 1s Wannier exciton (e.g., Ref. 17) and $M_x = \infty$ to bound excitons.[4] The exciton dispersion is

$$\hbar \omega_x(k) = E_x + \hbar^2 k^2 / (2 M_x), \tag{1}$$

where E_x is the exciton energy at zero wave vector. While it is useful to discuss semiconductors as a specific example, our considerations can be applied to any media with discrete linear optical resonances (they could, for example, be applied to semiconductor superlattices or even organic crystals). If the exciton has a nonzero spectral width of γ ($\gamma / \hbar$ is the dephasing rate), it follows from the general polariton dispersion relation $k^2 = \omega^2[n_b^2 + 4\pi\chi(\omega,k)]/c^2$ {where $\chi(\omega, k) = -\Gamma/[\hbar\omega - \hbar\omega_x(k) + i\gamma]$ is the susceptibility, Γ is the coupling strength, and n_b is the real background refractive index of the host material} that the polariton wave vector $k = k(\omega)$ is complex.

For $M_x = \infty$ (which we label as NSED for "no spatial exciton dispersion"), there is only one traveling polariton mode for each frequency,
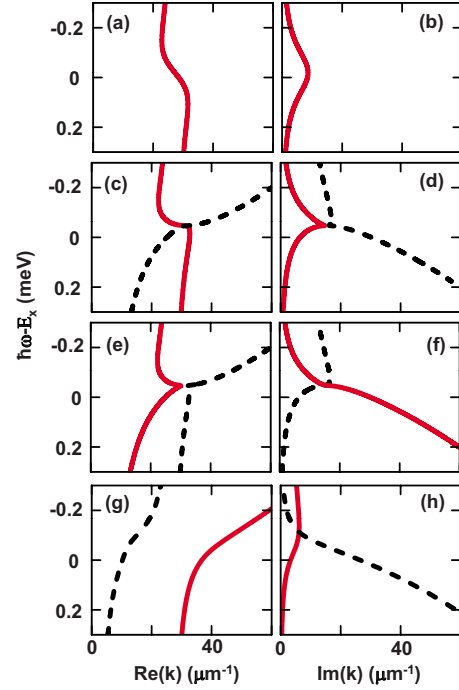

FIG. 2. (Color online) Calculated polariton dispersions {frequency vs real [(a), (c), (e), and (g)] and imaginary parts [(b), (d), (f), and (h)] of the wave vector k} without [NSED: (a) and (b)] and with [SED: (c)–(h)] spatial dispersion for dephasing rates of [(a)–(d)] $\gamma = 0.123$ meV, [(e) and (f)] $\gamma = 0.122$ meV, and [(g) and (h)] $\gamma = 0.050$ meV. Two disconnected noncrossing polariton branches appear in (e) and (g) where $\gamma < \gamma_0 = 0.12269$ meV, the critical dephasing rate, and their interference determines slow- and fast-light behavior. The materials parameters are: $\Gamma = 0.08$ meV, $n_b = 3.55$, $E_x = 1.5151$ eV and $M_x = 0.6 m_0$ (SED), $M_x = \infty$ (NSED).

$$k(\omega) = (\omega/c)\sqrt{n_b^2 + 4\pi\Gamma/(E_x - \hbar\omega - i\gamma)}. \tag{2}$$

Examples of the real (which yields the group velocity: $v_g^{-1} = n_g/c = d \, \mathrm{Re}[k(\omega)]/d\omega$) and imaginary [which gives the absorption coefficient: $\alpha(\omega) = 2 \, \mathrm{Im} \, k(\omega)$] parts of k vs ω are shown in Figs. 2(a) and 2(b). The transmission coefficient for the NSED is also known,[26] and for standard electromagnetic boundary conditions, is given by

$$T(\omega)e^{ik_0 L} = 4k_0 k/[(k + k_0)^2 e^{-ikL} - (k - k_0)^2 e^{ikL}], \tag{3}$$

where $k_0 = \omega/c$ is the wave vector in a vacuum. In the optically thick limit (OTL), i.e., $\mathrm{Im}[k(\omega)L] \gg 1$, this expression reduces to

$$T(\omega)e^{ik_0 L} = 4k_0 k e^{ikL}/(k_0 + k)^2. \tag{4}$$

For pulses that have a sufficiently narrow spectral width and/or a sufficiently small thickness L (cf. Sec V), the group velocity v_g is a valid concept, and the pulse envelope is transmitted undistorted in a transient time given by τ_g, where $\tau_g = L/v_g$.

In contrast, for $M_x < \infty$ (which we refer to as SED for with "spatial exciton dispersion"), there are two traveling polariton modes for each frequency (e.g., see Refs. 25 and 26),

$$k_{1,2}(\omega)^2 = \frac{M_x}{\hbar^2}\left[\left(\hbar\omega - E_x + i\gamma + \frac{\hbar^2\omega^2}{2M_xc^2}n_b^2\right)\right.$$
$$\left.\pm\sqrt{\left(\hbar\omega - E_x + i\gamma - \frac{\hbar^2\omega^2}{2M_xc^2}n_b^2\right)^2 + 8\pi\Gamma\frac{\hbar^2\omega^2}{M_xc^2}}\right],$$

$$(5)$$

whose group velocities and absorption coefficients are given by $v_{gi} = d\,\mathrm{Re}(k_i)/d\omega$ and $\alpha_i(\omega) = 2\,\mathrm{Im}\,k_i(\omega)$, respectively, where $i = 1, 2$. The real and imaginary parts of the dispersion for a SED polariton are shown in Figs. 2(c)–2(h) for three different dephasing rates.

In our discussions of SED polaritons, it is useful to define[27] a critical dephasing rate γ_0, at which there exists an ω such that $k_1(\omega) = k_2(\omega)$,

$$\gamma_0 \equiv \frac{M_xc^2}{n_b^2}\left(1 - \sqrt{1 - \frac{2E_xn_b^2}{M_xc^2}}\right)\sqrt{\frac{8\pi\Gamma}{M_xc^2}} \cong E_x\sqrt{\frac{8\pi\Gamma}{M_xc^2}}.$$

$$(6)$$

For dephasing rates larger than γ_0, one of the two branches is very similar to the single branch in the NSED case [compare the solid curve in Fig. 2(c) with Fig. 2(a)]. Since this branch also has a smaller absorption coefficient for all ω [Fig. 2(d)], most of the light transmitted through a sufficiently thick sample will propagate on this branch. Consequently, as with the NSED, spectrally narrow pulses are transmitted with their pulse envelopes undistorted in a time determined by the group velocity. Most previous studies have been performed in this regime.

However, if γ is slightly less than γ_0, the two $\mathrm{Re}(k)$ branches break up [Fig. 2(e)] with similar absorption coefficients around the breakup point [crossing of solid and dashed line in Fig. 2(f)]. As γ is reduced further, the separation between the two polariton branches, $\mathrm{Re}(k_1)$ and $\mathrm{Re}(k_2)$, increases [Fig. 2(g)], but the imaginary parts of the two branches cross [Fig. 2(h)]. In the region of this crossing, the propagation is not dominated by one branch or the other, and as we will discuss in the next section, *polariton interference* determines the slow- and fast-light characteristics. This interference should not be confused with that resulting from the transmission of polaritons in spatially anisotropic systems,[28] and with that resulting from different frequency components in a short pulse with a sufficiently broad spectrum.[29] The interference-based slow and fast light effects observed and analyzed in Refs. 28 utilize NSED systems that, because of birefringence, support polaritons with different polarization states. Below, we will show that interesting slow/fast light effects due to polariton interference are present in SED systems which are absent in *isotropic* NSED systems, and we delineate the parameter regimes for semiconductors where these effects could be observed.

The transmission coefficient for SED polaritons are also known.[26,30] Here, we use the simplest version of the additional boundary conditions[30] (ABCs) by setting the polarization wave to zero at the two ends of the slab. The more realistic exciton-free-layer generalization[31] of the ABCs does not change our findings qualitatively. The transmission coefficient under exciton-free-layer ABCs is provided in the Appendix. Using Pekar's ABCs, the transmission is given by[30]

$$T(\omega)e^{ik_0L}$$

$$= \frac{4k_0(\chi_2 - \chi_1)(N_{12} - N_{21})}{D(k_1, k_2) + D(-k_1, -k_2) - D(-k_1, k_2) - D(k_1, -k_2)},$$

$$(7)$$

where $\chi_i = \Gamma/(E_x + \hbar^2k_i^2/2M_x - \hbar\omega - i\gamma)$, $N_{ij} = \chi_i k_j(e^{ik_iL} - e^{-ik_iL})$, and

$$D(k, k') = e^{i(k+k')L}[\chi_2(k_0 - k) + \chi_1(k' - k_0)]^2 + 2kk'\chi_1\chi_2.$$

$$(8)$$

We refer to this exact expression for $T(\omega)$ as the "full" two-wave model in this paper. For $\mathrm{Im}[k_{1,2}(\omega)L] \gg 1$ (which we refer to as the "OTL" two-wave model), Eq. (7) becomes[26]

$$T(\omega)e^{ik_0L} = A(k_1, k_2)e^{ik_1L} + A(k_2, k_1)e^{ik_2L},$$

$$(9)$$

where the complex coefficient $A(k_i, k_j) = 4k_0k_i\chi_j(\chi_j - \chi_i)/[\chi_j(k_i + k_0) - \chi_i(k_j + k_0)]^2$. The coefficient A contains information about the boundary conditions. Close to the exciton resonance, where the absorption is large, the full and the OTL two-wave models yield almost identical results, and in this case, the simplicity of the OTL model makes its use advantageous.

It may be appropriate to point out that the transmission, Eq. (7), correctly accounts for the center-of-mass quantization of excitons.[27,31–33] But in the following discussion of bulk semiconductors, we mostly restrict ourselves to the OTL regime, where center-of-mass quantization is negligible.

III. TRANSIT TIME

Here, we discuss the slow and fast behavior of polaritons in terms of the experimentally measurable transit time $\bar{\tau}$, which is defined as the difference in times of arrival of the "center of mass" of the pulse at the back ($z = L$) and front ($z = 0$) surface of the sample,

$$\bar{\tau} = \frac{\int_{-\infty}^{\infty} t|E(t,L)|^2dt}{\int_{-\infty}^{\infty} |E(t,L)|^2dt} - \frac{\int_{-\infty}^{\infty} t|E(t,0)|^2dt}{\int_{-\infty}^{\infty} |E(t,0)|^2dt},$$

$$(10)$$

where the complex field is assumed to be of the form $E(t,z) = \mathcal{E}(t,z)\exp\{-i[\omega_0t - \mathrm{Re}(k)z]\}$, where ω_0 is the center frequency and $\mathcal{E}(t,z)$ the slowly varying amplitude. Using a spectral representation for the field amplitudes, $\bar{\tau}$ is found[34] to be the convolution of the transmitted pulse spectrum and the quantity $\tau(\omega)$,

$$\bar{\tau}(\omega_0) = \frac{\int_{-\infty}^{\infty} \tau(\omega)|E(\omega,L)|^2d\omega}{\int_{-\infty}^{\infty} |E(\omega,L)|^2d\omega} = \frac{\int_{-\infty}^{\infty} \tau(\omega)|\mathcal{E}(\omega - \omega_0,L)|^2d\omega}{\int_{-\infty}^{\infty} |\mathcal{E}(\omega - \omega_0,L)|^2d\omega},$$

$$(11)$$

where

$$\tau(\omega) = \mathrm{Im}[\partial \ln T/\partial\omega] = \mathrm{Im}[(\partial T/\partial\omega)/T] \qquad (12)$$

and

$$T(\omega) = E(\omega,L)/E(\omega,0)$$
$$= \exp[i\,\mathrm{Re}(k)L]\mathcal{E}(\omega-\omega_0,L)/\mathcal{E}(\omega-\omega_0,0) \qquad (13)$$

is the complex transmission coefficient given in the previous section. When the spectrum $|\mathcal{E}(\omega,L)|^2$ is much narrower than the features in $\tau(\omega)$, Eq. (11) becomes $\bar\tau(\omega_0)=\tau(\omega_0)$. For broader pulses, $\tau(\omega)$ is "smoothed" by the convolution with the pulse spectrum. In the next section, we will restrict our analysis to the narrow-band limit and discuss $\tau(\omega_0)$. The issue of spectrally broad pulses and spectral averaging will be addressed in Secs. V and VI.

IV. TWO-WAVE MODELS

An important observation in the context of slow and fast light is that for SED the transmission at a given frequency can be represented as a sum of two traveling polariton waves, $\exp[ik_1(\omega)L]$ and $\exp[ik_2(\omega)L]$. This is in contrast to the NSED case, where the transmission has only one factor, $\exp[ik(\omega)L]$. In this section, we will show numerical results calculated using the proper expressions for $T(\omega)$ for the full [Eq. (7)] and the OTL [Eq. (9)] two-wave models. However, for pedagogical purposes, we will find it convenient to discuss our results in terms of a model (referred to as the "simple" two-wave model) that ignores the details of the boundary conditions and that makes clear the role of polariton interference,

$$T(\omega) = e^{ik_1 L} + e^{ik_2 L}. \qquad (14)$$

One of the qualitative consequences of the "simple" two-wave model can be found straightforwardly from Eq. (12). At the frequency where both polariton branches experience the same absorption [$\mathrm{Im}(k_1)=\mathrm{Im}(k_2)$], the narrow-bandwidth transit time is

$$\tau(\omega_0) = (L/v_{g1} + L/v_{g2})/2 + \tan[\mathrm{Re}(k_1 - k_2)L/2]$$
$$\times \mathrm{Im}[\partial(k_1 - k_2)/\partial\omega]. \qquad (15)$$

For constructive interference between the two polariton modes at the end face $z=L$ [i.e., when $\mathrm{Re}(k_1-k_2)=2m\pi/L$, where m is an integer], Eqs. (14) and (15) show that the transit time $\tau(\omega_0)$ is equal to the *average* of the two transit times $\tau_{gi}=L/v_{gi}=n_{gi}L/c$ that would be obtained if the polariton wave were to simply propagate with the group velocity v_{gi}. In contrast, for destructive interference [i.e., $\mathrm{Re}(k_1-k_2)=(2m-1)\pi/L$, m an integer], $\tau(\omega_0)$ goes to infinity, consistent with a vanishing effective transit velocity (i.e., no light comes out). Below, we show that these and other characteristics of polariton interference and of the simple two-wave model are robust and are also present in the OTL and full two-wave models.

Figure 3 shows transit times (in the narrow-bandwidth limit) $\tau(\omega_0)$ for both the NSED and SED cases calculated using the OTL two-wave model (for three dephasing rates) in units of the transit time τ_0 in the absence of the excitonic resonance: $\tau_0=n_bL/c=L/v_0$, where $v_0=c/n_b$ is background
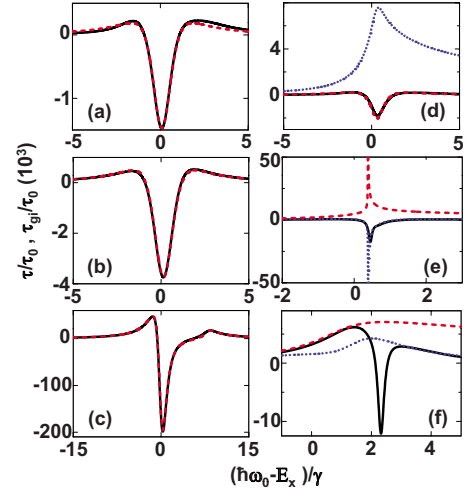

FIG. 3. (Color online) Comparison between the transit times $\tau(\omega_0)$ calculated using the OTL two-wave model (solid black line) and the transit times ($\tau_{gi}=L/v_{gi}=n_{gi}L/c$, where $i=1,2$) calculated using each group velocity (dashed red and dotted blue lines) for the [(a)–(c)] NSED and [(d)–(f)] SED cases for dephasing rates [(a) and (d)] $\gamma=0.2$ meV, [(b) and (e)] 0.123 meV, (c) 0.01 meV, and (f) 0.05 meV. The times are normalized by the transit time in the absence of the resonance: $\tau_0=n_bL/c$. For the [(a)–(c)] NSED, the solid (OTL) and dashed (τ_{gi}) lines are almost indistinguishable. $L=0.5$ μm and the material parameters are the same as in Fig. 2.

velocity. Also, plotted for comparison, are the transit times based on the group velocities, τ_{gi}. As expected, there is no discernible difference between the actual transit time $\tau(\omega_0)$ in the narrow-bandwidth limit and that based on the group velocity (τ_g) in the NSED case, Figs. 3(a)–3(c). Figures 3(a) and 3(b) show the familiar cases where γ is larger than the longitudinal-transverse splitting $\Delta_{LT}=4\pi\Gamma/n_b$. In these cases, the slow-fast-slow feature is almost symmetric with the fast light feature having spectral width comparable to the dephasing rate. In Fig. 3(c), where $\gamma<\Delta_{LT}$, the fast-light width is still approximately γ, but the slow-fast-slow structure is asymmetric (the fast light is at the resonance given by the transverse frequency, which is the exciton frequency).

By comparison, the transit times $\tau(\omega_0)$ in the narrow-bandwidth limit in the SED case [Figs. 3(d)–3(f)] show significant deviation from those calculated using a simple group-velocity approach, at least for $\gamma\lesssim\gamma_0$. For large dephasing, $\gamma>\gamma_0$, the transit time $\tau(\omega_0)$ coincides with the v_{gi} that is calculated using the group velocity of the one polariton branch that has the smaller absorption coefficient $\alpha_i(\omega)$. But if γ is close to or less than γ_0, $\tau(\omega_0)$ depends sensitively on the exact value of γ. In Fig. 3(e), γ is slightly larger than γ_0, and the τ_{gi} of each polariton branch becomes large (but with opposite signs) at the ω where $\mathrm{Re}(k_1)\cong\mathrm{Re}(k_2)$ [see Fig. 2(c)] and $\mathrm{Im}(k_1)\cong\mathrm{Im}(k_2)$ [see Fig. 2(d)], and $\tau(\omega_0)$ is approximately the arithmetic mean of τ_{g1} and τ_{g2}, in agreement with Eq. (15). But when $\gamma<\gamma_0$ [Fig. 3(f)], $\tau(\omega_0)$ is very large and negative, even though τ_{g1} and τ_{g2} are positive across the entire region near the exciton resonance. In other words, each group velocity is consistent with moderately slow slight but instead fast light is predicted. Clearly, in this regime, the transient time $\tau(\omega_0)$ is determined by po-
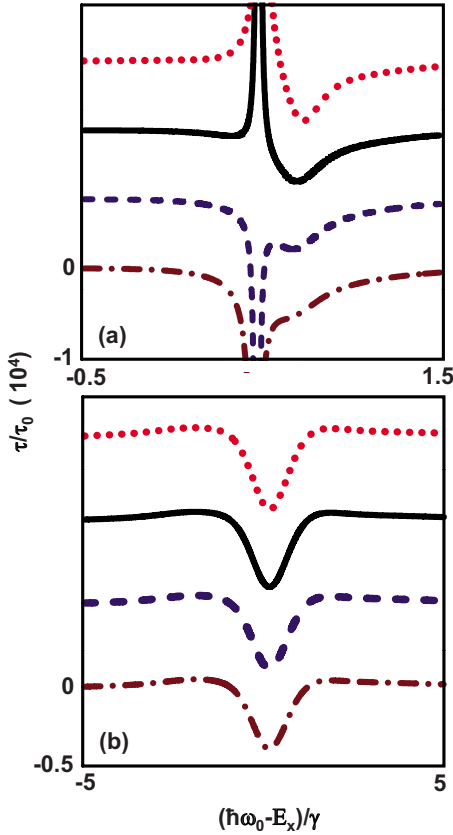
FIG. 4. (Color online) Transit times in the narrow-band limit $\tau(\omega_0)$ for (a) SED and (b) NSED for dephasing rates close to $\gamma_c(m=1)$: $\gamma=0.11$ meV (dotted red lines), $\gamma=0.115$ meV (solid black lines), $\gamma=0.117$ meV (blue dashed lines), and $\gamma=0.12$ meV (purple dashed-dotted lines). The curves are shifted vertically for clarity. The materials parameters are the same as used for Fig. 3.

lariton interference, not by the group velocities.

Equation (15) predicts singularities [i.e., infinite $\tau(\omega_0)$] when $\mathrm{Re}(k_1-k_2)$ approaches an odd multiple of π. Figure 4(a) shows $\tau(\omega_0)$ for the SED case calculated with the OTL two-wave model for several dephasing rates near one such singularity. The transit time undergoes a transition from a sharp fast-light peak to a sharp slow light peak by varying the dephasing only slightly. For comparison, Fig. 4(b) shows the corresponding $\tau(\omega_0)$ in the NSED case for the same four dephasing rates. In the latter case, all four curves exhibit similar approximately symmetric slow-fast-slow features, with the fast light feature having spectral width comparable to the dephasing rate. There is no sudden sharp transition from fast to slow.

The singularities that accompany the destructive interference between polariton modes are also illustrated in Fig. 5, where the maximum $\{\tau_{\max}(\gamma)=\max[\tau(\gamma,\omega_0)]\}$ and minimum $\{\tau_{\min}(\gamma)=\min[\tau(\gamma,\omega_0)]\}$ transit times are shown as a function of dephasing rate γ (where the maximization and minimization are performed with respect to ω in the vicinity of the exciton resonance). For the given material parameters, three values of γ are identified that produce destructive interferences and infinities in the transit times at frequencies, $\omega=\omega_c(m)$ with $m=1,2,3$ [these will be given in Eq. (17) below]. The exact positions of the slow-to-fast singularities
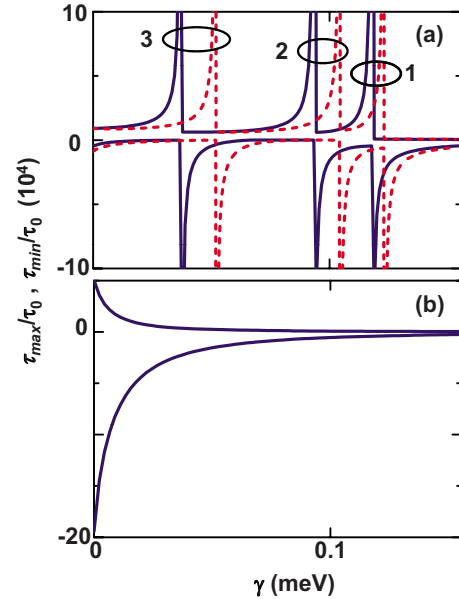

FIG. 5. (Color online) The maximum $\{\tau_{\max}(\gamma)=\max[\tau(\gamma,\omega_0)]\}$ and minimum $\{\tau_{\min}(\gamma)=\min[\tau(\gamma,\omega_0)]\}$ transit times determined for each dephasing rate γ as the center frequency ω_0 of the pulse is scanned across the exciton resonance for a (a) SED and (b) NSED—same materials parameters as in Figs. 2 and 3. The numbers 1, 2, and 3 indicate the values of m in Eq. (16). The solid lines show the full two-wave model and the red dashed lines the simple two-wave model. (The OTL two-wave model, not shown for clarity, is indistinguishable from the full model.)

in the simple two-wave model are slightly different from the full model but for the understanding of the qualitative features the simple model is sufficient. Notice that in the NSED case [Fig. 5(b)], the maximum and minimum transit times are finite for all $\gamma>0$, further illustrating that SED exhibits slow- and fast-light behavior as the result of polarization interference while NSED does not.

Approximate expressions for the dephasing rate γ_c and frequency ω_c at which the destructive interference shown in Fig. 5 occurs can be obtained (within the simple two-wave model) by applying the conditions $\mathrm{Re}(k_1-k_2)=(2m-1)\pi/L$ and $\mathrm{Im}(k_1)=\mathrm{Im}(k_2)$ to the known expressions for $k_1(\omega)$ and $k_2(\omega)$ given in Eq. (2). We find that there exist a finite number of discrete values of γ_c at which the transit time $\tau(\omega_0)$ goes to infinity, and for each γ_c, a single singularity occurs at a frequency ω_c. Explicitly, the sets of (γ_c,ω_c) at which the transit times become infinite are given by

$$\gamma_c(m) \cong E_x\sqrt{\frac{8\pi\Gamma}{M_xc^2}-\left[\frac{(2m-1)\pi n_b\hbar c}{LM_xc^2}\right]^2} \qquad (16)$$

and

$$\hbar\omega_c(m) \cong E_x + \frac{[\pi\hbar(2m-1)]^2}{2M_xL^2}, \qquad (17)$$

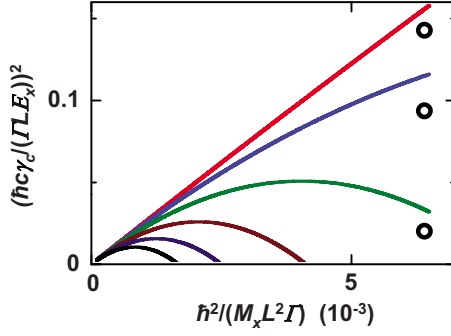where m is an integer bounded by the condition

FIG. 6. (Color online) The critical dephasing rates $\gamma_c(m)$ as a function of inverse mass M_x^{-1} calculated from the simple two-wave model, Eq. (16), for $m=1$ to $m=6$ (from top to bottom, respectively). The curves with larger values of m are ignored for clarity. The open circles show the positions of the singularities obtained in the OTL two-wave model for Fig. 5.

$$(2m-1)^2 \leq 8L^2 M_x \Gamma/(\pi n_b^2 \hbar^2). \tag{18}$$

Thus, if the dephasing rate γ can be varied, one can expect a finite number of singularities for a given sample, where E_x, M_x, L, and Γ are fixed. The number and location depend on the material parameters. When the actual values of (γ,ω) are close to one of the singular values $[\gamma_c(m),\omega_c(m)]$, one can expect $\tau(\omega_0)$, positive or negative, to be very long. This result is substantially different from the NSED case. For the NSED, any given γ leads to a $\text{Re}[k(\omega)]$ curve similar to the one shown in Fig. 2(a). Such a curve has two points where the group velocity $d[\text{Re}(k)]/d\omega \rightarrow \pm\infty$, in which case the transit times are zero. However, there is no point in the curve that allows for infinite transit times for $\gamma > 0$. In contrast, the SED case does allow for singularities ($\pm\infty$) in the transit time.

The well-known NSED model emerges from the more general SED case presented here in the following way. As $M_x \rightarrow \infty$, γ_0 and all $\gamma_c(m)$ go to zero, as indicated by Eqs. (6) and (16); hence $\gamma > \gamma_0$ for any nonzero dephasing, and the dispersion is dominated by one polariton branch [cf. Figs. 2(c) and 2(d)]. Also, inspection of Eq. (18), indicates that as $M_x \rightarrow \infty$, the number of singularities becomes large. Thus, we see that the NSED limit contains infinitely many singularities that are collapsed into a single point (namely, that of zero dephasing).

This collapse of $\gamma_c(m)$ to zero is illustrated in Fig. 6, where we plot $y = 8\pi x - [(2m-1)\pi n_b]^2 x^2$ with $y = [\hbar c \gamma_c(m)/(\Gamma L E_x)]^2$ and $x = \hbar^2/(M_x L^2 \Gamma)$, which follows from Eq. (16). We choose this way of plotting because the coefficients in the resulting equation depend only on n_b. Hence, any material with the same n_b is described by the same set of curves. The NSED material is represented by the vertical axis where M_x^{-1} is zero. Along this axis, i.e., varying the dephasing in the NSED case, we find no slow-to-fast light singularities, except at the point of vanishing dephasing. In the SED case, i.e., at positive values of the horizontal axis, we find a finite number of singularities for a given M_x^{-1}. As M_x^{-1} approaches zero, the number increases, and for clarity, the figure is restricted to $m \leq 6$. We also show the posi-

tion of the singularities obtained in the OTL two-wave model from Fig. 5 as open circles, which show only small deviation from the simple two-wave model.

V. FINITE BANDWIDTH

As we have shown in Sec. IV, in the case of media with spatial exciton dispersion, slow and fast light can be created by polariton interference, an effect absent in media without spatial dispersion. In the mathematical limit of sufficiently spectrally narrow pulses and for dephasing rates close to any $\gamma_c(m)$, this interference can lead to sharp features in $\tau(\omega_0)$ that have spectral widths much narrower than the width of the absorption resonance. In this section, we study finite pulse durations and find that the complex slow- and fast-light features resulting from SED can be resolved and distinguished from the NSED case. We also present quantitative criteria for virtually distortion-free pulse propagation in the spectral vicinity of these features. Such criteria have been developed for media without SED,[35,36] but are not applicable in the SED case. While SED offers a much richer variety of slow- and fast-light features than the well-known NSED case, the conditions necessary for observing these features are, in certain cases, much more stringent.

We write the transmitted pulse as the inverse Fourier transform of the transmitted spectrum,

$$E(t,L) = \int (d\omega/2\pi) \exp\{i[\varphi(\omega) - \omega t]\} E(\omega,0), \tag{19}$$

where the complex phase $\varphi(\omega) = -i \ln T(\omega)$. We then expand $\varphi(\omega)$ in a Taylor-series expansion to second order (assuming higher orders to be negligible) about the center frequency of the incident pulse, ω_0,

$$\varphi(\omega) \cong \varphi(\omega_0) + (\omega - \omega_0)\varphi'(\omega_0) + (1/2)(\omega - \omega_0)^2 \varphi''(\omega_0), \tag{20}$$

where all derivatives, denoted by primes, are with respect to ω. Using the notation $\Delta\omega \equiv \omega - \omega_0$ and $\varphi \equiv \varphi_r + i\varphi_i$, Eq. (19) can be rewritten in the form,

$$E(t,L) = \exp[-i(\omega_0 t - \varphi_r) - \varphi_i]$$
$$\times \int (d\Delta\omega/2\pi) \mathcal{E}(\Delta\omega,0) \exp\{-i\Delta\omega[t - \tau(\omega_0)]\}$$
$$\times \exp\left[i\frac{\Delta\omega^2}{\Delta\omega_{\text{GVD}}^2} - \left(\frac{\Delta\omega}{\Delta\omega_{\alpha 1}} + \frac{\Delta\omega^2}{\Delta\omega_{\alpha 2}^2}\right)\right], \tag{21}$$

where we make use of Eq. (12) to set $\varphi_r'(\omega) = \tau(\omega)$, note that $E(\omega_0 + \Delta\omega,0) = \mathcal{E}(\Delta\omega,0)$, and adopt the following definitions: $\Delta\omega_{\text{GVD}}^{-2} \equiv (1/2)\varphi_r''(\omega_0) = (1/2)(d\tau/d\omega)|_{\omega_0}$; $\Delta\omega_{\alpha 1}^{-1} \equiv \varphi_i'(\omega_0) = -\text{Re}[(d \ln T/d\omega)|_{\omega_0}]$; and $\Delta\omega_{\alpha 2}^{-2} \equiv (1/2)\varphi_i''(\omega_0) = (1/2)(d\Delta\omega_{\alpha 1}^{-1}/d\omega)|_{\omega_0}$. Notice that the output pulse envelope is an approximate replica of the input envelope, except delayed by $\tau(\omega_0)$, in the ideal limit where the pulse spectrum $\Delta\omega_p$ [full width at half maximum (FWHM) of the spectral intensity] is much less than the other characteristic spectral widths: $\Delta\omega_p \ll \Delta\omega_{\text{GVD}}, \Delta\omega_{\alpha 1}, \Delta\omega_{\alpha 2}$.

To obtain a physical appreciation for the quantities appearing in Eq. (21), it is useful to consider the limiting
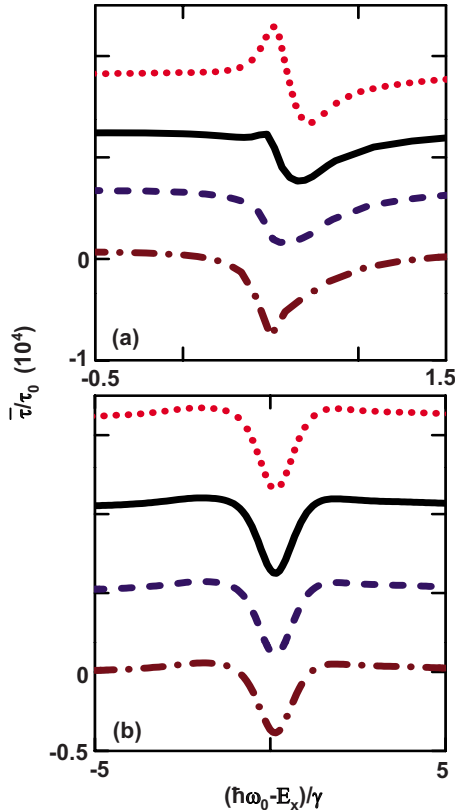
FIG. 7. (Color online) Same as Fig. 4 except for a finite pulse width of 100 ps. Actual transit times $\bar{\tau}(\omega_0)$ for (a) SED and (b) NSED for dephasing rates close to $\gamma_c(m=1)$: $\gamma=0.11$ meV (dotted red lines), $\gamma=0.115$ meV (solid black lines), $\gamma=0.117$ meV (blue dashed lines), and $\gamma=0.12$ meV (purple dashed-dotted lines). The curves are shifted vertically for clarity.

NSED case, where in the absence of boundary conditions, $T(\omega)=\exp(ikL)$. For the NSED, $\tau(\omega)=[d \, \mathrm{Re}(k)/d\omega]L$ is the group delay τ_g, and $d \, \mathrm{Re}(k)/d\omega$ is v_g^{-1}. Consequently, $\Delta\omega_{\mathrm{GVD}}$ is a measure of the group-velocity dispersion (GVD) and the two are related by $\Delta\omega_{\mathrm{GVD}}^{-2}=(L/2)(d^2 \, \mathrm{Re} \, k/d\omega^2)$ $=(-L/2v_g^2)(dv_g/d\omega)$. By comparison, $\Delta\omega_{\alpha 1}^{-1}=(L/2)(d\alpha/d\omega)$ and $\Delta\omega_{\alpha 2}^{-2}=(L/4)(d^2\alpha/d\omega^2)$ are determined by the frequency dependence of the absorption coefficient.

In Fig. 7, we show the transit time, $\bar{\tau}(\omega_0)$, of a 100 ps (FWHM of intensity) Gaussian optical pulse through both a SED and an NSED medium in the OTL two-wave model, using the same material parameters as in Fig. 4. In the narrow-bandwidth limit [Fig. 4(a)], the SED exhibits a spectrally narrow slow-to-fast light transition in $\tau(\omega_0)$ caused by polariton interference and corresponding to $m=1$ in the vicinity of $\gamma\approx 0.116$ meV. This transition is only present in the case with SED. Figure 7(a) illustrates that the smoothing of $\tau(\omega_0)$ by the convolution with the $\Delta\omega_p\cong 0.02$ meV spectrum of the 100 ps pulse prevents accurate resolution of the detailed features obtained in the narrow-band limit [Fig. 4(a)]. Nevertheless, this realistic bandwidth is sufficient to trace out identifiable attributes that result from the polariton interference. Moreover, a comparison of $\bar{\tau}(\omega_0)$ for the SED [Fig. 7(a)] and NSED [Fig. 7(b)] cases clearly shows the influence of the exciton dispersion. For the NSED case,
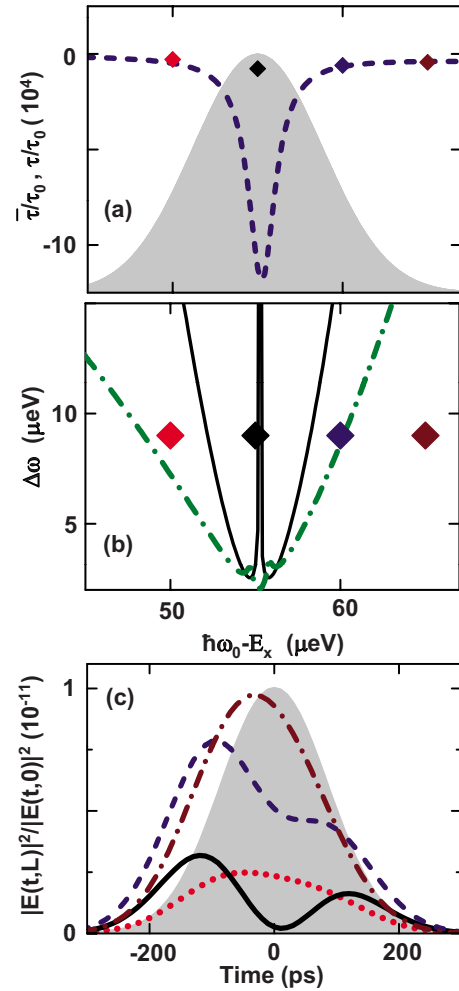

FIG. 8. (Color online) Illustration of the distortion experienced by a 200 ps pulse transmitted through a SED sample with γ $=0.117$ meV [see Fig. 4(a)] for four detunings. (a) The actual transit times $\bar{\tau}(\omega_0)$ and center frequencies ω_0 (marked by diamonds) are compared to delay times $\tau(\omega_0)$ in the narrow-band limit (navy dashed line). The spectrum (in arbitrary units) of the incident pulse is shown for comparison (gray shaded area). (b) The spectral distortion parameters, $|\Delta\omega_{\mathrm{GVD}}|$ (solid black curve) and $\Delta\omega_{\alpha}$ (dot-dashed green line), are compared to the actual spectral width $\Delta\omega_p$ at each center frequency ω_0 (again marked by diamonds). (c) The intensity profiles of the transmitted pulses for the detunings marked by diamonds in (a) and (b): $\hbar\omega_0-E_x=50$ μeV (red dotted), 55 μeV (black solid), 60 μeV (navy dashed), and 65 μeV (purple dot dashed). The incident temporal pulse profile (in arbitrary units) is also plotted for comparison (gray shaded area). The material parameters are the same as in previous figures.

$\Delta\omega_p \ll \gamma$ [the narrowest feature in $\tau(\omega_0)$], and the results for $\bar{\tau}(\omega_0)$ shown in Fig. 7(b) are practically indistinguishable from the narrow-band $\tau(\omega_0)$ shown in Fig. 4(b).

VI. PULSE DEFORMATION

In this section, we illustrate the deformation of pulses with finite bandwidth when they propagate near the sharp features associated with polariton interference. In Fig. 8, we

compare the distortions and actual delays, $\bar{\tau}(\omega_0)$, of a 200 ps pulse propagating near the $m=1$ fast-light polariton interference peak in a sample with $\gamma=0.117$ meV to their narrowband limits [i.e., to the dashed curve in Fig. 4(a)] for four different center frequencies ω_0 in the full two-wave model. In making these comparisons, we find it convenient to define $\Delta\omega_\alpha \equiv \text{minimum}\{|\Delta\omega_{\alpha 1}|, |\Delta\omega_{\alpha 2}|\}$. The key features are as follows: (i) when the center frequency of the pulse is tuned below (but near) the fast-light peak ($\hbar\omega_0 - E_x = 50$ μeV results in Fig. 8), $\Delta\omega_p < |\Delta\omega_{\text{GVD}}|$, but $\Delta\omega_p \sim \Delta\omega_\alpha$. Thus, the temporal profile of the pulse is mildly distorted by the higher-order derivatives associated with the absorption ($\Delta\omega_\alpha$) but the group-velocity dispersion contributes little. Under these circumstances, as mentioned above, the deviation of $\bar{\tau}(\omega_0)$ from $\tau(\omega_0)$ is dominated by the GVD term, which is small in this case. Thus, the pulse is advanced by an amount that is comparable to that predicted by the narrow-band limit [i.e., $\bar{\tau} \approx \tau \cong -2800\tau_0$].

(ii) In comparison, by tuning the pulse spectrum to the center of the fast-light peak ($\hbar\omega_0 - E_x = 55$ μeV), we find that $\Delta\omega_p \sim |\Delta\omega_{\text{GVD}}|$ and $\Delta\omega_p > \Delta\omega_\alpha$. The higher-order derivatives both of the absorption and of the dispersion combine to highly distort the pulse. Moreover, the convolution of the broader pulse spectrum $\Delta\omega_p$ with the narrow fast-light peak in $\tau(\omega_0)$ causes the magnitude of the latter to be greatly reduced and causes the pulse to be advanced much less than expected [$|\bar{\tau}| \ll |\tau(\omega_0)|$].

(iii) Next, the pulse is tuned above (but near) the fast-light peak ($\hbar\omega_0 - E_x = 60$ μeV). Here, the results are similar to the first case ($\hbar\omega_0 - E_x = 50$ μeV), where $\Delta\omega_p < |\Delta\omega_{\text{GVD}}|$ and $\Delta\omega_p \sim \Delta\omega_\alpha$. The pulse is distorted, primarily by the frequency-dependent absorption, and is advanced by $\bar{\tau} \approx \tau(\omega_0)$.

(iv) Finally, the pulse is tuned significantly away (above) from the peak in $\tau(\omega_0)$ to $\hbar\omega_0 - E_x = 65$ μeV. In this case, $\Delta\omega_p \ll \Delta\omega_\alpha < |\Delta\omega_{\text{GVD}}|$. As expected, the pulse is undistorted and advanced by an amount given by the narrow-band limit: $\bar{\tau} \cong \tau(\omega_0)$.

Notice that, while the advance of the pulse is many times the delay due to the background index τ_0 (in the range of $-3000\tau_0$ to $-8000\tau_0$) for each detuning, this delay is not a significant fraction of the pulse envelope. Moreover, a much longer pulse (with a narrower spectrum) would be needed in order to produce an undistorted transmitted pulse and to trace the sharp fast-light peak in the narrow-band limit. Such an example is shown in Fig. 9.

As proof of principle, Fig. 9 illustrates that a temporal (and spectral) pulse width can be chosen that satisfies the criterion for propagation without distortion (i.e., $\Delta\omega_p \ll \Delta\omega_\alpha, |\Delta\omega_{\text{GVD}}|$) for realistic materials parameters in a region where the pulse delay is not determined by the group velocity of either polariton branch but instead by polariton interference. Specifically, the figure shows a 500 ps pulse (having a 4 μeV spectral width) propagating near the same fast-light peak shown in Fig. 3(f) in the full two-wave model. In this regime, the time delay associated with each group velocity, $\tau_{gi} = L \partial \, \text{Re}(k_i)/\partial\omega$, is positive, but the predicted time delay is negative. When the finite pulse is tuned near this fast-light peak, it experiences a delay very similar to the predictions from the narrow-band limit [$\bar{\tau} \cong \tau(\omega_0) =$
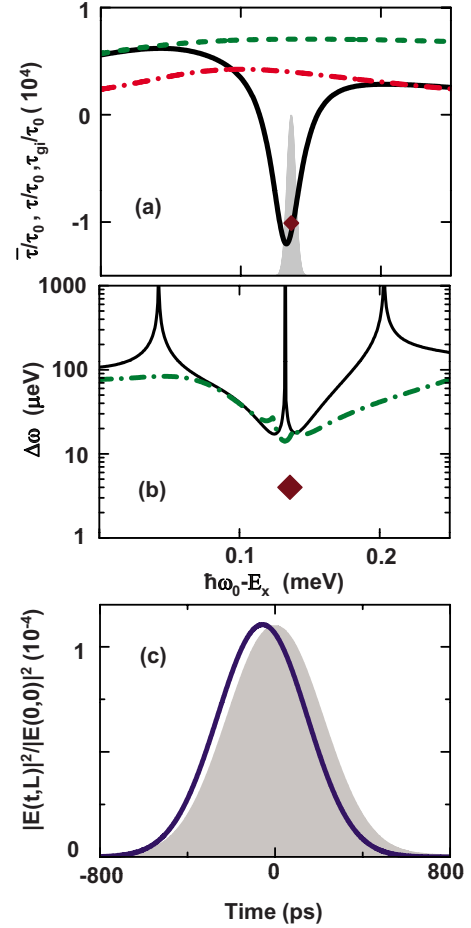

FIG. 9. (Color online) Demonstration of the distortionless transmission of a 500 ps pulse through a GaAs SED when the center frequency ω_0 is tuned to a sharp fast-light feature produced by polariton interference. (a) Enlarged view of Fig. 3(f), except that the actual transit time (marked by the diamond) is shown to be approximately equal to that predicted by the narrow-band limit (black solid line): $\bar{\tau}(\omega_0) \cong \tau(\omega_0)$. The spectrum (in arbitrary units) of the incident pulse is shown for comparison (gray shaded area). (b) The spectral width of the incident pulse $\Delta\omega_p$ (solid diamond) is shown to be less than the spectral distortion parameters, $|\Delta\omega_{\text{GVD}}|$ (solid black curve) and $\Delta\omega_\alpha$ (dot-dashed green line). (c) The intensity profiles of the transmitted (navy solid line) and incident (gray shaded area, arbitrary units) pulses are compared. The dephasing rate $\gamma = 0.05$ meV; otherwise the material parameters are the same as in previous figures.

-59.8 ps] without experiencing significant distortion.

The examples shown in Figs. 7–9 suggest that the criterion for the observation of slow- or fast-light features caused by polariton interference are rather stringent. Such experiments will require quality samples with dephasing rates below γ_0, the use of very long pulses with very small spectral widths, and the ability to measure delays with a resolution of a small fraction of a pulse width. In particular, in order for $\bar{\tau}(\omega_0) = \tau(\omega_0)$, the spectral widths of the pulses must be small enough to resolve any feature in $\tau(\omega_0)$. In the NSED case, this simply requires the spectral pulse width to be less than γ, and in the SED case, if $\gamma > \gamma_0$, the criterion is the same. If, however, $\gamma \leq \gamma_0$, the sharp features in $\tau(\omega_0)$ discussed above

must be resolved. The width of these features can be estimated by expanding $\tau(\omega_0)$ in the vicinity of the singularity $[\gamma_c(m), \omega_c(m)]$ to be,

$$\tau(\omega) = \frac{\hbar[\gamma_c(m) - \gamma]}{\hbar^2[\omega - \omega_c(m)]^2 + [\gamma_c(m) - \gamma]^2}. \qquad (22)$$

We see that, for a given γ, the pulse spectrum must be narrow compared to $\gamma - \gamma_c$. The closer that we tune toward γ_c; the more spectral resolution we need. Moreover, the number of singularities increases and their spectral separation decreases with increasing sample thickness [see Eqs. (17) and (18)]. For thick samples, it is very difficult to be tuned very far from a singularity.

To date, such experiments in SED structures have not been performed. Slow- and fast-light experiments have been performed in NSED semiconductor samples, e.g., near impurity transitions in doped semiconductors[4] and near the excitonic resonance in multiple quantum wells,[18] where spatial dispersion is not expected to be important. The observation of slow light in bulk material also has been reported,[17] in a regime where we estimate that the polariton interference effects discussed here might have been present, but none were seen. In their experiments, the authors[17] measured the delay of a 12 ps pulse through a bulk GaAs sample and observed a broad slow-light feature, but no fast light, as they tuned the center frequency across the excitonic resonance. Previously, it has been pointed out[36,37] that this experiment provides an excellent example of a situation where the convolution with relatively broadband pulses obscures the fundamental nature of the underlying polariton dispersion.

VII. CONCLUSION

In summary, we have shown that slow- and fast-light behavior in an absorptive medium depends strongly on the dispersion of the electronic resonance, parametrized by its effective mass M_x. Spatial exciton dispersion ($M_x < \infty$) allows for polariton interference, which in turn can make the transit time differ dramatically from the predictions based on the polaritons' group velocities. We have discussed the role of spectral convolutions between the finite spectra of pulses and these features in smoothing and spreading them for the case of media with spatial exciton dispersion. We conclude that it should be possible to observe these features and to distinguish media with spatial exciton dispersion from those without, provided the sample quality allows for an exciton dephasing less than the critical dephasing, which in the case of GaAs is found to be approximately 0.123 meV. Furthermore, we have presented quantitative criteria for distortionless pulse propagation in the spectral vicinity of slow- and fast-light features in semiconductors with spatial exciton dispersion. We hope that these results deepen the understanding

of slow and fast light in absorptive media, not only by clarifying slow and fast transit times in the $M_x < \infty$ case, but also by putting the well-known results of the $M_x = \infty$ case into broader context. Furthermore, we have restricted ourselves to the case of one absorptive resonance, but we expect nontrivial effects of polariton interference on slow and fast light in several other cases, for example, systems with multiple polaritons[38] (possibly including polariton continua), optically active polaritons, resonances involving exciton-biexciton transitions,[39] and inverted (gain) resonances.

APPENDIX: EXCITON-FREE-LAYER ADDITIONAL BOUNDARY CONDITIONS

To calculate the transmission coefficient in the SED case, we need to employ some additional boundary conditions. In this paper, we use a simplest ABCs, where the polarization is set to zero at the boundaries. Pekar's boundary conditions have been found[40] to give the best agreement with experimental data in the case of CdS. Recently, a generalization of Pekar's ABCs, namely, the exciton-free-layer ABCs, has been studied in great detail,[31] and only under very specific conditions of shallow exciton confinement, which is not the case of bulk GaAs samples, have they been found to be insufficient.[32] Here, front and back layers with thickness on the order of the exciton Bohr radius are kept free of excitons. The question arises whether our slow- and fast-light predictions depend sensitively on the specific form of the ABCs. In the case of the exciton-free-layers ABCs, the transmission coefficient is

$$T(\omega) = e^{-ik_0(d+L)}$$
$$\times \frac{16 k_0 k_d^2 (\chi_2 - \chi_1)(k_1 \chi_2 e^{ik_1(L-2d)} - k_2 \chi_1 e^{ik_2(L-2d)})}{(A_+ + A_-)^2},$$
$$(A1)$$

where d is the width of the exciton free layer, k_d is the wave vector in the exciton-free layer, $A_{+,-} = (k_d \mp k_0)[\pm k_d(\chi_1 - \chi_2) + (k_1\chi_2 - k_2\chi_1)]e^{\pm ik_d d}$. It can be seen that Eqs. (7) and (A1) both have a common factor $k_1\chi_2 e^{ik_1 x} - k_2\chi_1 e^{ik_2 x}$, where $x = L$ for zero-polarization boundary condition and $x = L - 2d$ for exciton-free-layer boundary condition. It is this factor that describes the polariton interference and that will lead to the singular behavior of the transit time. The difference in the effective width in the two ABC models is very small (for a sample thickness of 0.5 μm and a Bohr radius of 200 Å, it is 4%).

[1] R. W. Boyd and D. J. Gauthier, Science **326**, 1074 (2009).

[2] *Slow Light: Science and Applications*, edited by J. B. Khurgin and R. S. Tucker (CRC Press, Boca Raton, FL, 2008).

[3] L. V. Hau, S. E. Harris, Z. Dutton, and C. H. Behroozi, Nature (London) **397**, 594 (1999).

[4] S. Chu and S. Wong, Phys. Rev. Lett. **48**, 738 (1982).

[5] B. Segard and B. Macke, Phys. Lett. A **109**, 213 (1985).

[6] L. J. Wang, A. Kuzmich, and A. Dogariu, Nature (London) **406**, 277 (2000).

[7] M. D. Stenner, D. J. Gauthier, and M. A. Neifeld, Nature (London) **425**, 695 (2003).

[8] G. M. Gehring, A. Schweinsberg, C. Barsi, N. Kostinski, and R. W. Boyd, Science **312**, 895 (2006).

[9] N. G. Basov, R. V. Ambartsumyan, V. S. Zuev, P. G. Kryukov, and V. S. Letokhov, Sov. Phys. JETP **23**, 16 (1966).

[10] F. R. Faxvog, C. N. Y. Chow, T. Bieber, and J. A. Carruthers, Appl. Phys. Lett. **17**, 192 (1970).

[11] M. M. Kash, V. A. Sautenkov, A. S. Zibrov, L. Hollberg, G. R. Welch, M. D. Lukin, Y. Rostovtsev, E. S. Fry, and M. O. Scully, Phys. Rev. Lett. **82**, 5229 (1999).

[12] R. M. Camacho, M. V. Pack, J. C. Howell, A. Schweinsberg, and R. W. Boyd, Phys. Rev. Lett. **98**, 153601 (2007).

[13] S. Inouye, R. F. Low, S. Gupta, T. Pfau, A. Gorlitz, T. L. Gustavson, D. E. Pritchard, and W. Ketterle, Phys. Rev. Lett. **85**, 4225 (2000).

[14] M. S. Bigelow, N. N. Lepeshkin, and R. W. Boyd, Phys. Rev. Lett. **90**, 113903 (2003).

[15] K. Y. Song, M. G. Herráez, and L. Thévenaz, Opt. Express **13**, 82 (2005).

[16] Y. Okawachi, M. S. Bigelow, J. E. Sharping, Z. M. Zhu, A. Schweinsberg, D. J. Gauthier, R. W. Boyd, and A. L. Gaeta, Phys. Rev. Lett. **94**, 153902 (2005).

[17] R. G. Ulbrich and G. W. Fehrenbach, Phys. Rev. Lett. **43**, 963 (1979).

[18] S. Sarkar, Y. Guo, and H. L. Wang, Opt. Express **14**, 2845 (2006).

[19] M. S. Bigelow, N. N. Lepeshkin, and R. W. Boyd, Science **301**, 200 (2003).

[20] P.-C. Ku, F. Sedgwick, C. J. Chang-Hasnain, P. Palinginis, T. Li, H. L. Wang, S. W. Chang, and S. L. Chuang, Opt. Lett. **29**, 2291 (2004).

[21] H. Su and S. L. Chuang, Appl. Phys. Lett. **88**, 061102 (2006).

[22] A. Sommerfeld, Ann. Phys. **349**, 177 (1914); L. Brillouin, *ibid.* **349**, 203 (1914); The work of A. Sommerfeld and L. Brillouin is expanded, translated, and collected into a book: L. Brillouin, *Wave Propagation and Group Velocity* (Academic Press, New York, 1960).

[23] J. D. Jackson, *Classical Electrodynamics* (Wiley, New York, 1975).

[24] C. G. B. Garrett and D. E. McCumber, Phys. Rev. A **1**, 305 (1970).

[25] J. J. Hopfield and D. G. Thomas, Phys. Rev. **132**, 563 (1963).

[26] T. Skettrup, J. Phys. D: Appl. Phys. **14**, 1343 (1981).

[27] A. Tredicucci, Y. Chen, F. Bassani, J. Massies, C. Deparis, and G. Neu, Phys. Rev. B **47**, 10348 (1993).

[28] N. Brunner, V. Scarani, M. Wegmuller, M. Legre, and N. Gisin, Phys. Rev. Lett. **93**, 203902 (2004); D. R. Solli, C. F. McCormick, C. Ropers, J. J. Morehead, R. Y. Chiao, and J. M. Hickmann, *ibid.* **91**, 143906 (2003).

[29] J. S. Nägerl, T. Reker, G. Böhne, and R. G. Ulbrich, Phys. Status Solidi B **206**, 357 (1998).

[30] S. I. Pekar, Sov. Phys. JETP **34**, 1176 (1958).

[31] H. C. Schneider, F. Jahnke, S. W. Koch, J. Tignon, T. Hasche, and D. S. Chemla, Phys. Rev. B **63**, 045202 (2001).

[32] S. Schumacher, G. Czycholl, F. Jahnke, I. Kudyk, H. I. Rückmann, J. Gutowski, A. Gust, G. Alexe, and D. Hommel, Phys. Rev. B **70**, 235340 (2004).

[33] M. Seemann, F. Kieseling, H. Stolz, G. Manzke, K. Henneberger, and D. Hommel, Solid State Commun. **138**, 457 (2006).

[34] J. Peatross, S. A. Glasgow, and M. Ware, Phys. Rev. Lett. **84**, 2370 (2000).

[35] Md. Aminul Islam Talukder, Y. Amagishi, and M. Tomita, Phys. Rev. Lett. **86**, 3546 (2001).

[36] M. Tanaka, M. Fujiwara, and H. Ikegami, Phys. Rev. A **34**, 4851 (1986).

[37] P. Halevi, in *Spatial Dispersion in Solids and Plasmas*, edited by P. Halevi (Elsevier Science, Amsterdam, 1992), Chap. 6.

[38] G. Fishman, Solid State Commun. **27**, 1097 (1978).

[39] S. Chesi, M. Artoni, G. C. La Rocca, F. Bassani, and A. Mysyrowicz, Phys. Rev. Lett. **91**, 057402 (2003).

[40] W. Stössel and H. J. Wagner, Phys. Status Solidi B **89**, 403 (1978).